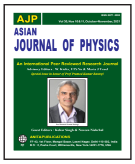

Asian Journal of Physics
Vol. 30, Nos 10 & 11 (2021) 1547-1572
Available on: www.asianjournalofphysics.com

ap

Micro and nano scale optical metrology for shiny surfaces and difficult to access aircraft engine components – A review

Aswin Haridas[1, 2, 3,] and Murukeshan Vadakke Matham[1, 2*]

[1]*School of Mechanical and Aerospace Engineering, Nanyang Technological University, Singapore 639798*

[2]*Centre for Optical and Laser Engineering, 50 Nanyang Avenue, Singapore 639798*

[3]*Testia GmbH, an Airbus company, Cornelius-Edzard-Straße 15 – 28199 Bremen, Germany*

Dedicated to Prof Pramod Kumar Rastogi for his outstanding contributions to Optical Metrology

Industrial production has always been driven by global competition and the need for efficient market adaptation. A strategic initiative termed Industry 4.0 was recently introduced to cater to these demands, which increased the requirements for both the manufacturing and the metrology sectors. It is predicted that the futuristic aircraft engines would contain large components with microscale features and those having areas that are difficult to access or complex internal channels. While the former requires dedicated measurement systems that challenge the physical limitations of optics, the accessibility of the latter set of components poses additional challenges. This paper provides an overview of the *State-of-the-Art* literature survey conducted in the related research fields. Various techniques for evaluating surface roughness parameters of rough and shiny surfaces (0.2 μm < Ra < 25 μm) are investigated. The outcome of the literature review is thereafter summarized, which leads to identifying the key research gaps in the domain.

Keywords: Surface roughness evaluation, optical imaging, non-destructive optical techniques, Industry 4.0, Factory of the future, Aircraft engine components, Aerospace inspection.

1 Introduction

Air traffic statistics of passenger movements can be used to study the population choosing airline travel over conventional means [1]. To efficiently manage the growing passenger statistics, manufacturing initiative in-line with Industry 4.0 aims to revolutionize the aerospace sector by integrating business strategies and specialized processes. Industry 4.0 is supported by nine technological pillars, namely, autonomous robots, 3D simulations, horizontal and vertical system integration, the internet of things (IoT), cyber security, cloud computing, additive layer manufacturing (ALM), augmented reality and big data analytics [2]. Among these advancements, ALM (or 3D printing) has been widely investigated by aircraft manufacturers around the world. In addition to materials such as carbon fiber composites [3,4], shape memory alloys [5] and aerogels [6], ALM has transformed the aviation industry by improving the mechanical properties and design flexibility of critical components. Therefore, the aerodynamic efficiencies and structural efficiencies of the components can be enhanced. However, the metrology advancements are not on par with the rising demands of the manufacturing sector.

The motivation for this paper arises from the need to identify the characteristics of metrology systems for the factories of the future. In this paper, four critical requirements for developing the next generation of metrology systems are identified (for Inspection 4.0), namely, data visualization, system automation,

Corresponding author
e mail: mmurukeshan@ntu.edu.sg (Murukeshan VM)*; asw_hari@yahoo.com* (Aswin Haridas)

data handling for closed-loop operation and measurement system applicability. Figure 1 illustrates these requirements.

From Fig 1, automation and machine-machine collaboration are identified as the primary requirement Inspection 4.0. The connected systems would then have to work cohesively to generate data sets (e.g., point cloud) that require handling and preprocessing before extracting information. These connected systems can be achieved by implementing machine learning and artificial intelligence (AI) algorithms. Further, the use of augmented reality and virtual reality creates an interactive and immersive measurement experience. All the characteristics must be component-independent to ensure that the operation costs are minimized. Based on these factors, new implementation strategies for developing measurement systems are envisaged for futuristic aerospace components.

The futuristic aircraft engine components can be characterized by large surface areas (up to few meters or more) with microscale features (such as the metallic and composite fan blades) and those having areas that are difficult to access or complex internal channels (e.g., aircraft fuel nozzles manufactured using ALM) [7]. In the case of the former, the use of traditional contact-based surface roughness evaluation techniques resulted in surface contamination and increased measurement time. Additionally, the lateral resolution for far field non-contact optical measurement techniques for areal roughness measurements is limited by the Abbe diffraction limit.

Fig 1. Inspection 4.0 – future metrology [8].

Alternatively, for the latter, apart from developing metrology systems, attributes such as probe accessibility and locomotion are also of importance [8]. Although commercial endoscopic tools are suitable for visual inspection of these areas, these techniques are not suitable for quantitative surface roughness evaluation. In this context, it can be inferred that the development and advancement of new materials and processes are not entirely matched by the capabilities developed for characterizing them. In this paper, we review the state-of-the-art techniques for evaluating surface roughness parameters of rough and shiny surfaces (0.2 μm < Ra < 25 μm). The available literature is classified into three sections. Primarily, the first section investigates speckle-based techniques described in ISO 25178 under the areal integrating methods. Techniques based online profiling and areal topography evaluation are discussed in the second section, considering the prospects of industrial requirements for surface roughness evaluation. The third section evaluates the capabilities of the discussed techniques for surface roughness evaluation of areas that are difficult to access and internal channels. Also, the limitations of the borescope and endoscope inspection probes are detailed.

2 Surface profile measurements and areal surface roughness evaluation

For over a century, surface profile methods, such as stylus profilers have been vastly employed for surface roughness evaluation of aerospace components due to its ability to determine the extent of manufacturing process change [9,10]. Especially for the aircraft engine manufacturing sector, line parameters, specifically Ra, is used as the golden standard. However, for stochastic surface roughness evaluation, which entails manufacturing processes such as ALM, these methods fail to provide relevant information about the functional capabilities of the surface under test [8]. Figure 2 (a) shows a reference specimen having a periodic surface structure. Surface profile measurements and areal surface roughness measurements over a region of interest (rectangular area in (a)) are shown in Fig 2 (b) and Fig 2 (c), respectively. Even though surface profile measurements can estimate the periodicity of the surface features, it fails to characterize cracks and burrs obtained from areal methods (shown in Fig 2 (c)) which could affect the component functionality.

The past few decades have, therefore, seen an increase in the use of areal surface roughness evaluation techniques for problem diagnostics and functional prediction of surfaces in academic research. However, manufacturing industries still rely on the incomplete measurements provided by surface profilers as they are easy to implement and well-established. In this context, the next few sections review various technologies for evaluating surface roughness parameters that can improve the current aerospace manufacturing processes.

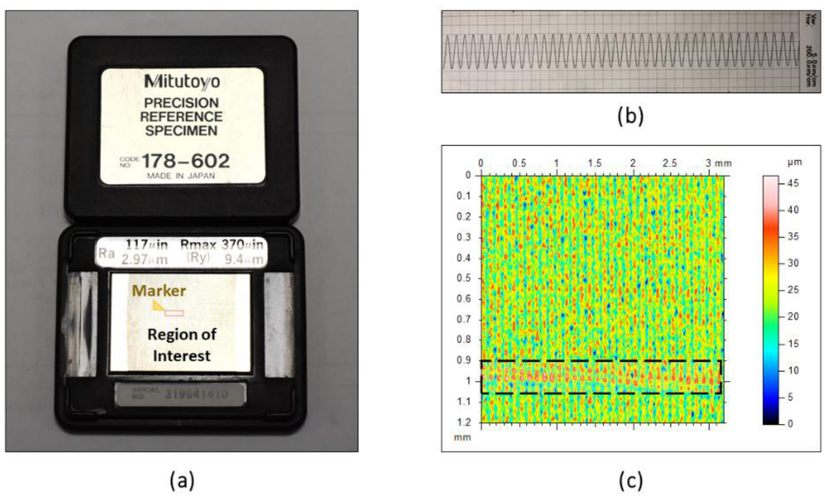

Fig 2. The surface profile and areal surface roughness of a reference specimen with periodic surface structure (a) are shown in (b) and (c), respectively [8].

2.1 Surface roughness measurement instruments - classification

As per the ISO 25178 part, 6 (2010), surface roughness evaluation techniques can be classified into three sections, as shown in Fig 3 [10].

The line profiling instruments such as the contact-based stylus produces a 2D plot of the surface height distribution, which can be mathematically represented by a height function $z(y)$. On the other hand, areal topography methods produce a 3D topographical image of the surface represented by $z(x, y)$. The surface roughness parameters can be evaluated from the 3D surface topography. In contrast to line profiling and areal topography methods, areal-integrating methods only provide a statistical representation of the surface under study. Although, several techniques are included within each of these classes, the scope is limited to those techniques that are capable of evaluating surface roughness parameters from rough and shiny (0.2 μm < Ra < 25 μm) aircraft engine components.

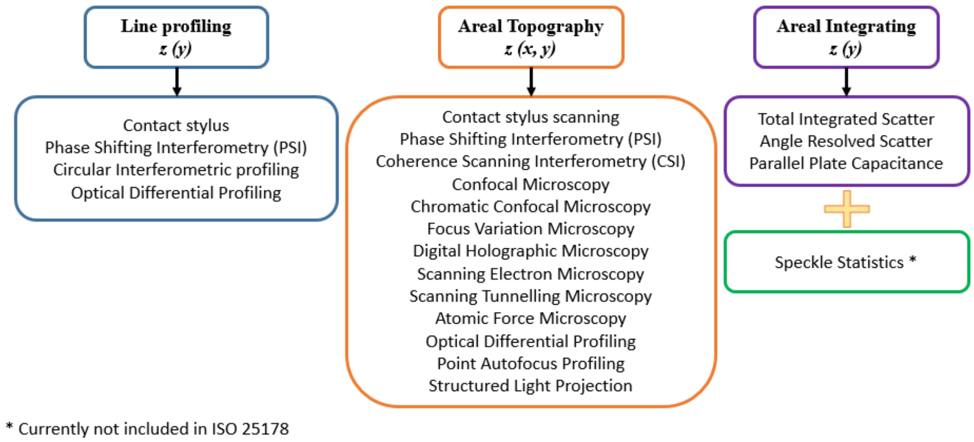

Fig 3. Types of surface roughness measurement methods as per ISO 25178 (Adapted from [8])

2.2. Evaluating surface roughness parameters - Areal integrating methods

Since the earliest applications of optics, it was understood that smooth surfaces and rough surfaces scatter light in different ways. Areal-integrating methods evaluate the surface roughness parameters by analyzing the scattered light from the surface of an object taking advantage of this difference. An overall surface roughness parameter is then calculated for a chosen measurement area. Angle-resolved scatter (ARS), and total integrated scatter (TIS) are two of the most used techniques for surface roughness evaluation that make use of this principle. While the former deals with measurement and analysis of scattered light at various orientations with respect to the sample, the latter captures and inspects light that is not specularly (mirror-like) reflected [10]. Commonly, the optical configuration of ARS consists of a continuous-wave laser (or lamp) that illuminates the specimen [11]. The reflected light is captured using a detector mounted onto a goniometer. ARS has been widely used for the measurement of surface roughness in the range of a few Å [10,11-16]. ARS necessitates a highly sensitive detector in addition to a vacuum environment to achieve high measurement accuracies [10,11,14]. These constraints increase the overall cost and measurement time. TIS, on the other hand, uses Ulbricht spheres or Coblenz spheres to collect the scattered light (20 to 850) [17,18]. Similar to ARS, TIS prefers a cleanroom environment for high measurement accuracies. Although both ARS and TIS are popular for evaluating surface roughness parameters from smaller components such as silicon wafers, they are not suitable for the analysis of large structures due to the constraints imposed by the optical instrumentation [19]. In addition, the need for sample preparation, environmental restrictions, and relatively higher cost reduces its applicability for industrial applications [18,20-14]. In this context, the next few sections investigate the ability of speckle-based areal-integrating techniques to overcome the disadvantages of ARS and TIS.

2.2.1 Speckle Metrology

The term speckle refers to a random granular appearance observed when a highly coherent beam (e.g., from a laser source) illuminates an optically rough surface, such as a piece of paper, white paint, a display screen, or a metallic surface [25-30]. Speckles are generated only if a monochromatic (coherent) source illuminates a surface with height variations in the order of, or greater than the wavelength of the illumination source. When such a surface is illuminated, the complex amplitude of light at any point in space is given by the superposition of the amplitudes described by a set of vectors having a random phase. So, due to the surface height variation, the net resultant amplitude and phase vary from point-to-point, generating a speckle pattern [31]. Conventionally, the generated speckle pattern can be classified into two broad categories, namely, objective speckle patterns and subjective speckle patterns. Objective speckle patterns are generated when a coherent source illuminates an optically rough surface, and the intensity of the scattered light is collected onto an observation plane without an imaging lens. Unlike an objective speckle pattern, a subjective speckle pattern is a result of imaging the surface being illuminated onto an observation plane using an imaging lens [31,32]. Figure 4 (a) shows a subjective speckle pattern generated from an optically rough surface. Figures 4 (b) & 4 (c) show the optical arrangement for generating objective and subjective speckle patterns, respectively.

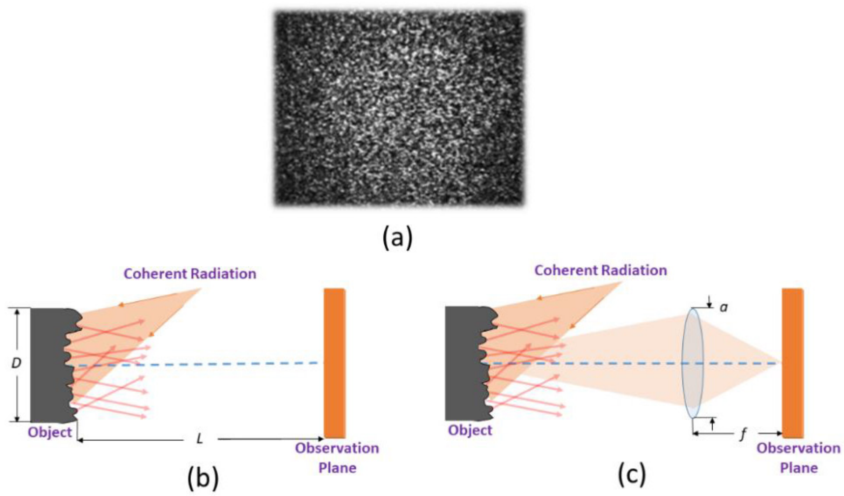

Fig 4. Conventional speckle pattern generated by illuminating an optically rough surface with a coherent source is shown in (a). Optical arrangement for objective and subjective speckle pattern generation is shown in (b) and (c), respectively [8].

Since the invention of the lasers in the early 1960s, there have been many interests in developing speckle techniques for surface metrology. Initially regarded as a noise that can affect the image quality significantly, it was later understood to be an explicit sensor to glean surface topographic information. Since then, laser speckles have been widely used for applications that demand surface quality checks. Recent developments in specialized optical components have revived the interests in using speckle techniques for in-line applications [28,33-39].

The first order statistics of speckles, alternatively termed as the speckle contrast, is one of the properties that vary with surface roughness. The analysis determines the contrast of the speckle pattern formed in the far field of an imaging system. In general, contrast is defined as the difference in luminance that makes an object distinguishable. In statistical optics, speckle contrast is defined as the ratio of standard deviation (σi) of the intensity to the average intensity $\bar{I}$ of the speckle pattern. Furthermore, this method can be termed as the measure of how strong the fluctuations of intensity are in a speckle pattern compared to the average intensity. For a fully developed speckle pattern, the speckle contrast, C' is given by Eq (1) [27].

$$C' = \frac{\sigma i}{\bar{I}} \tag{1}$$

A speckle pattern has a high contrast, if [40]

a) the interfering waves have a sufficient phase difference ($> \frac{\lambda}{2}$) to produce a completely destructive interference at some points on the speckle pattern and,

b) the interfering beams are temporally coherent with each other.

The first condition explains why the speckle contrast is low for relatively smooth surfaces, while the second condition describes the need for a laser-based illumination system. However, if a spatially coherent light having a broad spectral bandwidth is used for illumination, the second condition would be partially valid. A number of researchers have calculated the average surface roughness parameter, Ra using speckle contrast and compared with the contact based profilometers [26,29,41,42]. It was observed that the surface roughness parameters could not be relied on if the surface under investigation has a short coherence length. Also, the measurement range is limited to ~ $\lambda/4$ for normal coherent illumination on the surface [41]. Even though speckle contrast analysis is capable of measuring the average surface roughness parameter, Ra, the measurement range of the system is limited for inspecting rough and shiny (0.2 µm < Ra < 25 µm) aircraft engine components.

The second order speckle statistics, i.e., speckle correlation, have been investigated for evaluating surface roughness parameters. Two speckle patterns recorded one after the other are partially correlated if the speckle statistics are slightly modified by changing the orientation of the component (or illumination) or varying the speckle size. Necessary conditions for correlating two speckle patterns include [30,37,41,43],

a) RMS surface roughness is greater than the wavelength of the coherent source.
b) Fully developed speckles (contrast equals 1) are formed.
c) The surface height probability distribution is Gaussian.
d) Shadowing, multiple reflections, and volume scattering are neglected (surface is isotropic and homogeneous).

The degree of correlation depends on several factors, including, the surface geometry, surface translations/rotations, and the speckle size. Two of the most common speckle correlation techniques used for evaluating surface roughness parameters are angular speckle correlation and spectral speckle correlation.

Angular speckle correlation utilizes the dependency of the speckle pattern on the orientation of the sample or the illumination source. A correlation factor, *C*, is obtained from two speckle patterns which are simultaneously captured from the same sample area that is illuminated by two coherent plane waves at two different angles of incidence. The correlation factor, *C*, is related to the root-mean-square roughness parameter, *Rq* by the following relationship,

$$C = \exp\left(-\left(\frac{2\pi}{\lambda \sin\theta_1 \delta\theta_1}\right)^2\right) \tag{2}$$

here, θ_1 is the incidence angle, and $\delta\theta_1$ is the deviation angle. Generally, the correlation factor is less than one as the two speckle patterns recorded by the imaging camera are not fully correlated.

A large number of researchers have demonstrated the capability of evaluating surface roughness parameters using ASC [44-46]. Léger and Perrin measured samples having an average surface roughness between 1 µm and 30 µm using a quasi-automatic ASC setup in less than 30 seconds [44]. Spagnolo *et al* verified ASC by measuring standard samples with an average roughness between 4 µm and 31 µm [45]. Toh *et al* extended the measurement range by rotating the sample instead of the illumination beam. The measurement system was validated using standard roughness samples with an average surface roughness between 1.6 µm and 50 µm [46]. Persson presented the mathematical model of ASC, which was validated by measuring samples with an average surface roughness between 1 µm and 10 µm [37].

In contrast to ASC, spectral speckle correlation exploits the relationship between the wavelength of the illumination source and the size of the individual speckle. Ruffling observed that the degree of correlation between two speckle patterns recorded on the same surface by two different wavelengths also depends upon the surface quality [47]. In this case, the theoretical equation governing the relationship between the degree of correlation, C, and the RMS surface roughness can be written as,

$$C = \exp\left(-\left(\frac{4\pi\Delta\lambda}{\lambda_1\lambda_2} R_q \cos\theta\right)^2\right) \tag{3}$$

Here, the degree of correlation is related to the RMS roughness, the incidence angle, θ, the wavelengths λ_1 and λ_2, and the difference in wavelengths, $\Delta\lambda$, respectively.

Persson measured the measurement range of SSC, both theoretically and experimentally. For a visible illumination source, the range of SSC was found to be confined between 0.5 µm < Ra < 5 µm. He also reported the sensitivity of the method towards misalignments and vibrations [43]. To further improve the measurement range, Bernd and Jürgen theoretically and experimentally estimated the dependence of SSC on partially developed speckle patterns. Under the assumption of a large number of scattering cells, the surface roughness parameters of surfaces with wavelengths smaller than the illumination wavelength were measured [48]. Recently, Spagnolo extended the measurement range of SSC by incorporating a wavelength tunable laser with fine-tuning capabilities [49].

2.3. Areal topography measurement instruments - Classification

Based on the principles of operation, the dominant source of noise and measurement uncertainties, areal surface topography evaluation techniques can be divided into three broad categories, namely, interferometry, deflectometry, and triangulation-based systems. The principle of data acquisition and processing technique also varies with the category.

2.3.1 Interferometry-based techniques

Interferometry-based techniques include classical phase measuring interferometers such as phase shifting interferometry (PSI) and coherence scanning interferometry (CSI) for smooth surface inspections and speckle-based interferometers for rough surfaces (a modified CSI). While the former evaluates the phase of the interference pattern, the latter evaluates the first and second order statistics of the observed speckle patterns to determine the surface topography characteristics.

2.3.1.1 *Phase Shifting Interferometry* (PSI) was developed to determine surface topographic information from a large field at a long WD from both shiny and rough components [51]. It is one of the most established techniques for surface topography measurements. PSI uses an interference objective in combination with known phase shifts to demodulate the interference data into 3D surface topography [50].

Modern interference microscopes employ removable interferometric objectives to provide more flexibility and convenience (e.g. employing a Michelson, and Mirau interferometric objectives). The WD and magnification of the optical arrangement are entirely dependent on the design of the objective lens. Michelson interferometric objectives are used for applications that require lower magnifications (less than 10X). Due to the ease in manufacturing, Mirau interferometric objectives are used for applications that require higher magnifications (between 20× and 100×).

2.3.1.2. *Coherence Scanning Interferometry* (CSI), also known as white light interferometry (WLI), evaluates the surface topography either using infrared or visible-light (mostly white light). CSI has been used for the measurement of surface roughness, step heights, and surface discontinuities due to its broad measurement range (from tens of nanometers up to a few centimeters) [12].

The working principle of CSI is similar to PSI. However, in contrast to the PSI, the fringes formed in CSI can only be observed over a narrow height range. The changes in the fringe patterns are used to evaluate the surface topography. A source with a broadband spectrum is used to illuminate the pupil plane of the interferometric objective. Stable interference fringes (with high contrast) are formed at the detector due to a long coherence length. An aperture stop and a field stop controls the NA and the FOV, respectively. Also, using a vertical scanner, fringes can be recorded at various z locations [12,53]. Being an established technique, CSI is used for applications including semi-transparent thin films [54], storage disk drives [55], solder inspection, and machined surfaces [12,56].

2.3.1.3. Digital holographic microscopy (*DHM*): In contrast to PSI and CSI, DHM evaluates the surface roughness parameters from a single image. Being a holographic technique, DHM uses a two-step architecture, (i) acquiring the hologram and (ii) reconstructing the 3D surface topography from the hologram. A DHM system consists of a coherent illumination source, an interferometer, a detection camera, and an image processing unit. Even though a coherent illumination source is preferred for DHM, sources having a lower coherence have been implemented in several studies to reduce speckle noise [57,58]. The choice of the interferometer used mainly depends upon the sample chosen. Typically, to evaluate the surface roughness parameters of a reflective sample, a Mach-Zehnder interferometer or a Michelson interferometer is used due to the ease in alignment [59].

Multiple applications employ DHM for real-time (~ 20 frames per second (fps)) surface roughness evaluation [59]. For micro-optics applications, DHM is used to characterize the micro-surface topography and micro-defects. Being well established, DHM is also used for various research applications. Kühn *et al* used an aerospace test-target to measure the range of DHM [60,61]. In this case, an adequate stitching algorithm and phase offset adjustments were used.

2.3.2 Deflectometry-based techniques

Deflectometry-based techniques for surface topography evaluation determine the slope of the surface under inspection. For macroscopic surfaces, a periodic grating pattern is placed at a remote distance from a sample which acts as a mirror. A charge-coupled device (CCD) captures the reflection of the pattern from the sample. The distortion of the reflected pattern is studied to evaluate the surface topography. This technique was first implemented by Ritter and Hahn using Moiré reflection gratings [62]. For shape measurements on specular free-form surfaces, phase analysis using deflectometry was introduced by Knavery *et al* [63]. Deflectometry is used for multiple industrial applications including shape measurements [63] and defect detection [64] of aspheric glasses and car windows. The use of longer illumination wavelengths [65] and portable devices [66] are suggested to improve the measurement range and the measurement speed, respectively.

High-resolution deflectometry or micro-deflectometry was proposed to evaluate surface roughness parameters [67]. Unlike its macroscopic alternative, micro-deflectometry uses a microscopic objective lens for high-resolution imaging. Although the FOV is limited to 100 μm, SEM-like surface topography images are obtained [68]. Here, an electronically controllable spatial light modulator generates the periodic grating patterns. These patterns are projected onto the sample using a microscopic objective. The same microscopic objective captures the reflected image of the pattern [67].

2.3.3 Triangulation-based techniques

Techniques for surface topography evaluation based on triangulation include laser triangulation, fringe projection, focus variation, confocal microscopy, chromatic confocal microscopy, and SIM [10]. A conventional triangulation-based measurement system uses a laser source which is focused onto the sample surface. The reflected pattern is captured using a CCD sensor. The triangulation angle, θ' represents the angle enclosed by the illumination and detection vectors. Knowing the location of the laser spot on the CCD sensor, surface height variation $z(y)$ can be calculated [70].

For optically rough surfaces (surface with height variations in the order of, or greater than the wavelength of the illumination source), triangulation-based systems are severely affected by speckle noise. The observation aperture is chosen to be smaller than the illumination aperture to reduce the speckle noise [69]. In addition, by employing illumination sources with low temporal coherence, the speckle noise can be further reduced [71].

The measurement uncertainty for triangulation-based techniques is a function of θ'. However, in the case of focus variation microscopy and confocal microscopy, the measurement uncertainty is defined based on the NA of the microscopic objective lens [72]. Here, the investigation is limited to focus variation microscopy, confocal microscopy, and SIM for high-resolution surface topography evaluation of rough and shiny surfaces.

2.3.3.1. Focus variation microscopy

A focus variation microscope uses microscopic objective lenses of small DoF to vertically scan the sample surface (in ~ μm steps) to evaluate the 3D surface topography. Due to its ability to measure steep slopes, focus variation microscopy has been used for surface texture and surface form measurements of rough and shiny surfaces [73-75]. The necessary components of a focus variation microscope include an illumination source, a CCD camera for detection, optical components with a limited DoF, and a vertical scanning unit. Collimated light from a white light-emitting diode (LED) source is focused onto the sample surface using a microscopic objective lens. Depending on the surface topography, the light beam reflects in different directions. A part of this light is collected by the objective lens, which is captured by the CCD camera. In the case of a diffuse reflection from the sample surface, the reflected light would be scattered in all directions. Whereas, in the case of a specular reflection, the light energy would be concentrated in the direction of the specular reflection. Further, based on the axial location of the objective lens (with respect to the sample surface), the reflected light is focused onto the detector at different angles [10,74]. Therefore, by moving the sample along the axial direction, the degree of focus (given by the intensity of the reflected light captured by the CCD) changes from low to high and then back to low again [10]. By analyzing the degree of focus from the captured images, the surface topography of the sample is obtained. Focus variation microscopes have been implemented for various applications being commercially available. Applications including surface form measurement on the cylindrical part of contour artifact and 3D topography of drill bits and thread cutters use focus variation microscopes for inspection [73,74]. In order to accurately measure components with large surface areas, modifications to the lateral scanning scheme and innovative illumination designs have been proposed [74]. However, in order to use focus variation microscopes to obtain the 3D surface topography, the height variations on the sample surface should be sufficiently large (depends on the microscopic objective lens used). Also, the CCD sensor must be capable of resolving small intensity variations.

2.3.3.2. Confocal microscopy

Introduced by Minsky in 1957, the confocal microscope is one of the most powerful tools for 3D surface profiling and imaging [75,76]. A confocal microscope employs a spatial pinhole at the confocal plane of a lens system to eliminate the background (out-of-focus) light and increase the imaging resolution. In comparison to the optical techniques that use a high NA microscope objective lens, a confocal microscope has multiple advantages such as, a high lateral resolution and a high measurable slope [77-79].

A typical confocal microscope consists of an illumination source, a CCD detector, a beam splitter, two aperture stops, and a microscopic objective lens. The light from the point source is projected onto the focal plane of the microscopic objective lens after passing through an aperture located at the field diaphragm of the optical microscope. Therefore, at the focal plane of the objective lens, a diffraction-limited illumination spot is obtained. At the conjugate plane of the illumination pinhole, a second aperture is positioned so that the photo-detector records a high signal only when the surface is placed at the focal plane of the microscopic objective lens. When the surface is not at the focal plane of the microscopic objective, the photo-detector records a lower signal. Further, to evaluate the 3D surface topography, an axial scan of the sample surface is required [80]. Usually, a confocal microscope uses an objective lens with high NA, which further suppresses the unwanted background reflection due to a small DoF. Several variations of the confocal microscope have been proposed for evaluating 3D surface topographies [77,81].

Typically, a confocal microscope is used for, (i) horizontal measurements using a high-resolution intensity map and (ii) 3D measurements using a height map. The microscope must be periodically calibrated to ensure high measurement accuracy. Since the shape of the beam at the focal plane of the microscopic objective affects the accuracy and repeatability of the measurements, the illumination spot must be calibrated so that it remains within the critical limits. The measurement accuracy of the horizontal (x-y) and vertical (z) axes driving mechanisms must also be calibrated to avoid positional errors. The lateral resolution and the axial resolution of the confocal microscope are dependent on a combination of linear guides, feeding screws, and pulse motor leads [82]. A Nipkow disk having multiple pinholes is used to inspect a larger surface area. Typically, in a Nipkow disk, the diameter of a pinhole is 20 μm (spaced out in x-y plane at 200 μm intervals; spiral arrangement). By uniformly illuminating the Nipkow disk, multiple scanning sources are formed on the specimen surface [81]. This arrangement is used to scan the x-y plane. In addition, scanning mirrors, arrays of microlenses, and digital micro-mirror devices (DMD) have been used to replace the Nipkow disc [79,84].

In comparison to a stylus profiler, confocal microscopy provides faster image acquisition and sub-micron resolution in a large FOV [79]. Also, the measurement parameters, including WD, lateral resolution, and FOV, are dependent on the choice of the microscopic objective lens.

2.3.3.3. Structured illumination microscopy (*SIM*)

Structured illumination microscopy is a high-resolution imaging technique used to evaluate surface topography parameters of rough and shiny engineering components. In principle, a sinusoidal fringe pattern is projected onto the specimen surface through a microscopic objective lens. Depending on the surface topography of the specimen under test, the projected pattern would reflect or scatter. The modulated fringe pattern is then imaged onto the detector through the same microscopic objective for 3D surface topography evaluation.

Initially developed by Engelhardt and Häusler in 1988 [85], 3D surface topography evaluation using SIM was further improved by Neil *et al* [86] and Wilson [87]. However, the method did not gain popularity until Gustafsson *et al* implemented a SIM for biological applications demonstrating a two-fold improvement in the lateral resolution [87]. Although several implementations of SIM have been discussed in the literature, super resolution-SIM (SR-SIM) and optical sectioning-SIM (OS-SIM) are most widely used [69,88-98].

The concept of lateral resolution improvement using SR-SIM can be well understood using the Moiré effect. Here, the sample is illuminated using a set of structured illumination patterns that modulates the reflected light to generate Moiré fringes. Knowing the position (phase) and orientation of the illumination pattern, the sub-diffraction structures on a sample can be recovered from these Moiré fringes [90]. Unlike SR-SIM, OS-SIM differentiates the in-focus and out-of-focus areas on a sample surface to improve the lateral resolution and the optical sectioning ability. For an in-focus plane and an out-of-focus plane, the contrast of the Moiré fringes generated using the same set of structured illumination patterns would be different. Since the out-of-focus plane areas are not modulated by the structured illumination patterns, the contrast of the Moiré fringes generated would be ~ 0. Therefore, high-resolution images of the in-focus planes can be generated by removing the structured illumination patterns from the reflected images [94]. OS-SIM has been used for optical sectioning and high-resolution imaging applications due to the ease of implementation and low data processing requirements. For biological applications, Gustafsson *et al* [87-89] and Saxena *et al* [99] describe the various implementations of OS-SIM and SR-SIM. However, only a few modifications to the OS-SIM configuration have been suggested for engineering applications [100-102]. Artigas *et al* used a set of multiple thin lines to illuminate the sample surface instead of the conventional sinusoidal patterns. By measuring the intensities of the reflected lines, the 3D surface topography of an engineering sample was evaluated. Compared to OS-SIM using sinusoidal illumination patterns, the imaging resolution and the measurement speed were observed to be improved. Also, different algorithms have been proposed to evaluate the 3D surface topography, including, fringe phase shifting [79] and spatial convolution [100]. An adequate phase shifting algorithm was implemented for the former to detect focus variations based on fringe contrast. However, the latter used a conventional spatial convolution algorithm to evaluate the 3D surface topography. Being a methodology based on triangulation, surface topography evaluation of optically rough surfaces using SIM suffers from speckle noise [70]. The measurement uncertainty for surface height evaluation of rough surfaces is comparatively higher than smooth surfaces due to the presence of speckle noise. For optically rough surfaces, the measurement uncertainty for surface height evaluation is proportional to ~ $1/NA^2$. In contrast for optically smooth surfaces, the measurement uncertainty for surface height evaluation is dependent on the photon noise associated with the imaging system. In addition, the spatial frequency of the projected sinusoidal pattern also affects the measured height uncertainty [94]. In this case, the measurement uncertainty is proportional to ~ $\lambda/(NA^2 \times SNR)$.

Table 1 provides a summary of line and areal surface topography techniques for evaluating the surface roughness parameters of rough and shiny surfaces.

Table 1. Summary of line and areal surface topography techniques for inspecting rough and shiny surfaces (0.2 μm < Ra < 25 μm).

Measurement Technique	Axial and Lateral Resolution	Measurand	Advantages	Limitations
Stylus Measurement	**Axial**: Sampling method **Lateral**: Depends on the tip radius and surface heights	Surface roughness Waviness and form (Line Scan/ area)	* Applicable for rough and shiny surfaces * Relatively easy operating principle * High measurement reliability and traceability * Well established ISO standard	* Long measurement time for large area inspection * Surface indentations due to probe contact * Probe deflections and skid * Affected by sampling errors and environmental noise * Errors in data processing * Finite stylus dimensions
SEM	**Axial and Lateral Resolution:** - Imaging step size - Electron beam diameter (~5 nm)	Surface topography	* Applicable for rough and shiny surfaces * Large DoF and depth of focus * Well established ISO standard	* Long measurement time for large area inspection * Contamination due to charge build-up * Need for specimen preparation * Small measurement area and working distance * 2D inspection/ specimen tilt for 3D imaging * Vacuum required

SPM (AFM)	**Axial**: Sampling method (0.1 nm) and fine positioning system **Lateral**: Tip radius and surface height [2-10 nm]	Surface topography	* Used for applications where the surface amplitudes are much smaller than the typical limits of the stylus. * Measurement range up to a few tens to hundreds of micrometer square	* Contaminates the specimen surface (in contact mode) * Long time for easurement * Area of the order of a few square micrometers * Not suitable for in-line measurements
Interferometric Techniques for Surface Topography Evaluation				
Phase Shifting Interferometry (PSI)	**Axial** and **lateral** resolution in nm	Surface topography	* High axial and lateral resolutions * 3D surface topography * Applicable for topography inspection of shiny surfaces	* Incapable for rough surface inspection due to speckle noise * Need for mechanical scanning and thereby, long measurement time * Accuracy depends on the quality of the reference surface * Hardware complexities due to focus requirements * Errors due to detector nonlinearity, phase shifting and phase unwrapping.
Coherent Scanning Interferometry (CSI) or WLI	**Axial**: ~ 3 nm **Lateral**: ~ 1 µm	Surface topography	* High-resolution imaging * Established ISO standards * Being interference-based; independent of NA and FOV	* Multiple error sources - periodic surface texture - step discontinuities - sensor signals - environment noise * Not for sloped surfaces and complex geometries
Digital Holographic Microscopy (DHM)	**Axial**: ~ 0.1 nm **Lateral**: Diffraction limited	Surface topography	* Fast (µ seconds) and real-time measurements (20 fps) * High vertical and lateral resolution * High DoF due to digital focusing * Requires mechanical scanning * Insensitive to vibration (in-line measurements)	* Presence of parasitic interference and statistical noise (Due to off-axis geometry for real-time imaging) * Maximum measurement height $\lambda/2$- reflection and λ in transmission 2π modulo algorithm * Not suitable for rough samples due to speckle noise

Measurement Technique	Axial and Lateral Resolution	Measurand	Advantages	Limitations
Deflectometry Technique for Surface Topography Evaluation				
Deflectometry	**Axial and lateral resolution:** in nm	3D surface topography	* High-resolution surface form and roughness measurements for specular surfaces * Large DoF	* Relatively new technique for surface topography * Not applicable for rough surfaces * Theoretical limitations due to speckle and photon noise
Triangulation Techniques for Surface Topography Evaluation				
Focus Variation Instruments	**Axial** (~ 10 nm) and **lateral resolution**: Objective lens dependent (www.ALICONA.com)	Surface topography (form and roughness)	* High DoF * High axial and lateral resolutions * 80° maximum slope (independent of objective NA)	* Large measurement time; small FOV * Resolution is objective lens dependent * Need good focus variation on the sample * Affected by environmental noise
Confocal Microscopy	**Axial**: Nanometers **Lateral**: Sub-micron	Surface topography	* Fast, non-contact and non-destructive * Higher image contrast due to background image subtraction (pinhole) * 3D coordinate reconstruction * Analysis of samples with slopes	* Low signal power; pinhole screening * Labor intensive * Objective lens dependent (FOV and WD)- diffraction limit * Errors due to mechanical scanning and environmental noise
Chromatic confocal microscopy	**Spot size**: 5-10 µm for vertical range < 1 mm 10-20 µm for > 1 mm **Axial:** Sampling methods (nanometers) **Lateral**: Sub-micron (dependent on spot size)	Surface topography	* Non-contact substitute for the stylus instruments * Scan length dependent on an *x-y* stage * Used for curved surfaces * Insensitive to ambient light and stray reflections * In comparison with confocal does not require an axial scan * Lesser noise due to vibration	* Inspection of a sample with incline; light escapes the objective lens * Scanning speed depends on translation stage and data acquisition frequency * Measurement outliers depends on the intensity of light received on the detector

Structured Illumination Microscopy (SIM)	**Axial**: NA dependent **Lateral**: Diffraction limited imaging	3D surface topography	* Applicable for both rough and smooth surfaces (low noise-incoherence) * High lateral resolution and WD; diffraction limited imaging * FOV is objective lens dependent * Fast "on the fly" measurements solder inspection * Large DoF and higher angular range of slope measurements * Low complexity in configuration * Possible in-line inspection system	* Relatively new thus less established * Theoretical limitations due to speckle and photon noise

2.4. Miniaturized probes for surface roughness evaluation

In general, the probes used for measuring the surface roughness parameters of components located at hard to access areas can be divided into three categories based on their principle of operation, (i) rigid non-optical probes, (ii) rigid optical probes and (iii) flexible optical fiber-based probes. The conventional stylus probe is an example of a rigid non-optical probe. Figure 5 (a) shows the schematic diagram of a conventional stylus probe with an extended stylus tip. Although these probes have been used for surface roughness measurements of internal channels with straight pathways, their capability is dependent on the physical dimensions of the stylus instrument. Therefore, to improve the accessibility of the measurement equipment, rigid optical probes were investigated. One of the most common examples of a rigid optical probe is a rigid borescope (and rigid endoscope). Figure 5 (b) shows the schematic diagram of a rigid optical borescope.

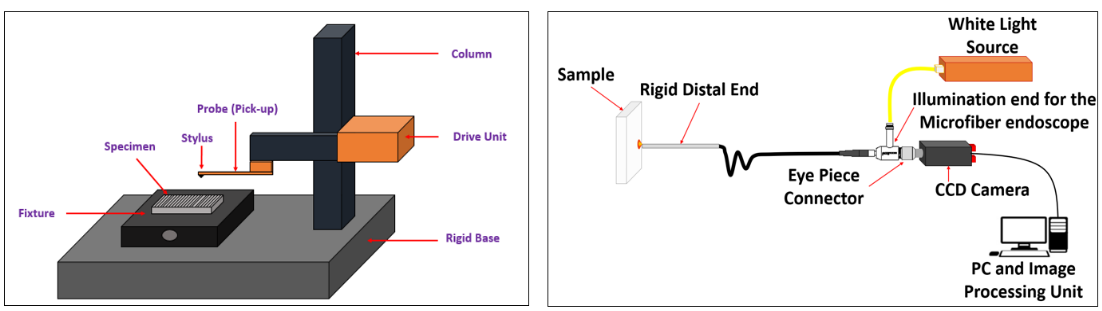

a) b)

Fig 5. Schematic diagram of (a) a conventional stylus probe and (b) a rigid optical borescope.

These probes have been used for engineering applications for visual inspection of critical components. However, the lack of flexibility and the inability to evaluate quantitative information have limited their applications. In addition, the minimum achievable diameter of the probe is limited due to the presence of bulk optics at the distal end. Hence to address these issues, flexible, easily maneuverable, optical fiber-based probes have been used. An imaging optical fiber probe bundle consists of up to ~100,000 individual single mode optical fibers with diameters ranging between ~80 µm up to several millimeters [101]. Since the relative arrangement of the individual fibers is consistent throughout the length of the bundle, images are transmitted in a pixelated form. These optical fiber bundles have been used to reduce the complexities of the distal end of an imaging probe, thereby offering smaller probe diameters and bending radii [102,103].

Due to the inherent flexibility of the optical fiber bundles, these fibers have also been used in various fields of optical imaging that includes, flexible borescopes, flexible endoscopes [101], CSI [104], coherence domain-imaging [105], optical coherence tomography (OCT) [106], and confocal microscopy [107]. However, these applications necessitate specialty optical fiber with expensive optical components [108]. Figures 6 (a and b) show the schematic diagram of a conventional flexible borescope and an optical-fiber based CSI. Figure 7, compares various features of the commercially available optical fiber-based probes in the market.

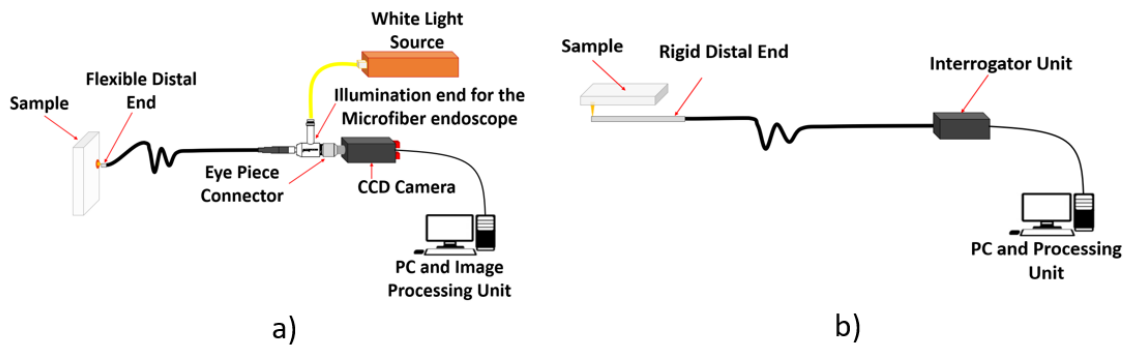

Fig 6. Schematic diagram of (a) a flexible borescope and (b) an optical fiber-based CSI.

Product/ Features	Hawkeye® Flexible Video Bore scopes	Fujifilm Fiber Optic Endoscope (FB Series)	Olympus IF series video probes	Novacam Technologies	GE XL Vu Utility Video Probes
Depth-of-Field (mm)	3 – 10	5-50	5-10	4-15	4-12
Scope Diameter (mm)	4-20	4-5	5-9	3-100	2.4- 6
Insertion Tube Bend Radius (mm)	10-40	30-40	20-30	30-40	32
Field/Direction-of-View	~ 50º	~ 120º	~ 100º	~ 50º	~ 90º
Side-View Tip	YES	YES	YES	NO	YES
Category/Suitability	Medical Video Endoscope	Medical Video Endoscope	Industrial Video bore scope and Medical Video Endoscope	Industrial Profilometer	Industrial Video bore scope

Fig 7. Comparison of commercially available flexible probes for NDT of areas hard to access and complex internal channels

Apart from probe flexibility, adequate parametric design of the distal end lens system is essential to implement optical image fiber-based probes for the inspection of components that are located at areas hard to access or internal channels. In addition, suitable image processing algorithms must be developed to evaluate the surface roughness parameters from these areas. Although several optical fiber-based probes have been investigated for the inspection of components located at areas hard to access, evaluating the quantitative surface roughness parameters from these components is still a challenge, therefore, there is a critical requirement in designing optical fiber-based imaging system for a fast, non-contact and non-destructive evaluation of surface roughness parameters.

3 Ongoing Research: Micro and nano scale optical metrology for shiny surfaces and difficult to access aircraft engine components

Taking into consideration the identified gaps in the technologies for inspecting shiny surfaces and difficult to access aircraft engine components, some of the ongoing research activities at the Center for Optical and Laser Engineering (COLE), Nanyang Technological University include, but are not limited to, (a) investigation into speckle based techniques for inspecting areal surface roughness of shiny surfaces & difficult to access areas, (b) evaluation of surface roughness parameters using high resolution surface imaging at long working distances and (c) investigation into optical fiber probe based solutions in order to evaluate areal surface roughness parameters from difficult to access aircraft engine components and internal channels. Some of the key research outcomes are described as follows.

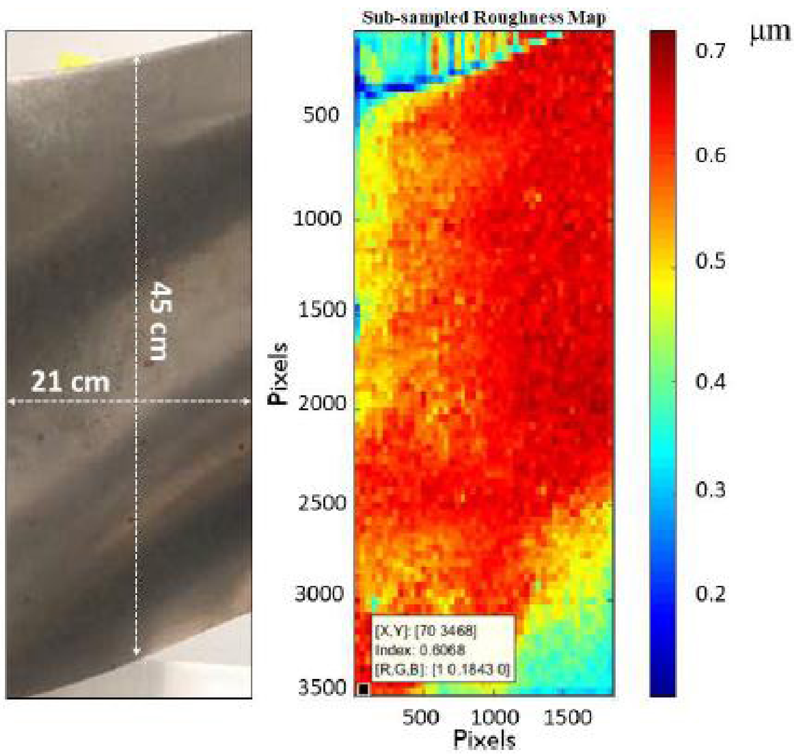

Fig 8. Illuminated area of an aerospace engine component and the sub-sampled roughness map (Color bars indicate the calculated sub-sampled average surface roughness) [8]

Speckle-based techniques including speckle contrast analysis, speckle correlation analysis, and speckle image analysis are being investigated for evaluating surface roughness parameters of large areas with micro-scale features. From the initial theoretical simulations and experimental validations, a measurement range ~ 0.2 μm < Ra < 0.6 μm was achieved using speckle contrast [109]. Although implementing speckle contrast measurements in an industrial setting is relatively simple, the measurements were found to be affected by environmental noise. Angular Speckle Correlation (ASC) was, therefore, investigated to overcome the shortcomings of speckle contrast. Even though ASC was found to be well established for evaluating surface roughness parameters, theoretical simulations had determined the following disadvantages for the inspection of shiny aerospace components (0.2 μm < Ra < 0.6 μm), (i) the dependence of ASC with $\boldsymbol{\delta}\theta_1$ would require precise rotations to achieve the desired measurement range and (ii) the relationship between $\boldsymbol{\delta}\theta_1$ and the specimen twist results in additional errors. For line side inspection of large structures with micro-scale features, the measurement range achievable (limited by choice of $\boldsymbol{\delta}\theta_1$) was ~ 5 μm < Ra < 25 μm [110].

In order to obtain the desirable surface roughness measurement range necessitated by shiny aircraft engine components, Spectral Speckle Correlation (SSC) techniques have also been investigated. For SSC, a measurement range of 0.2 μm < Ra < 0.6 μm was theoretically calculated and experimentally validated [111]. An automated optical system was developed for evaluating surface roughness parameters of large structures having micro-scale features. The proposed system contains optimized imaging and illumination sub-systems to ensure robustness and compactness. A 60 mm×45 mm FOV can be captured in one shot with minimal measurement errors. To measure a 10 mm×10 mm area, SSC took 1/15th the time taken by conventional techniques [112,113]. Figure 8 shows the surface roughness (sub-sampled) map determined using the developed system. The tests were conducted on an aircraft engine component.

One of the drawbacks of using SSC is that the technique requires two speckle images in order to determine the correlation factors. This would mean that the factors including specimen displacement and backlash errors affect the surface roughness measurements. Therefore, we also investigate binary image analysis algorithms to differentiate surface roughness based on captured speckle images. The speckle patterns are converted into a binary image with thresholds estimated from the image histogram. By observing the variations in component connectivity and component size, surface roughness can be differentiated [115,116].

Although speckle imaging techniques have been found to be effective in estimating a statistical coefficient related to the areal surface roughness, they are unable to calculate the real surface roughness parameters. The research conducted, therefore, was also extended to the development of high-resolution imaging techniques at long working distances.

Two microscopic configurations, namely, Structured Illumination Bessel beam Microscopy (SIBM) and structured illumination embedded speckle microscopy have been developed & are being investigated for high-resolution surface imaging of rough and shiny components at long working distances. A novel SIBM microscope, capable of high-resolution far field reflection imaging with the sub diffraction resolution, combines the advantages of Bessel Beam Microscopy (BBM) and SIM to improve the imaging resolution. A Siemen’s star chart was used as the test sample to numerically estimate the lateral resolution of SIBM in the reflection configuration. Using a 50X NIKON TU Plan ELWD corrected long WD microscope objective (50X, NA 0.55, 11 mm WD), the lateral resolution of a SIBM was calculated as 505 ± 5 nm. In comparison, the lateral resolution of a conventional microscope (without the SIM and BBM unit), an OS-SIM (without the BBM unit; using an LC-SLM) and a standard laser scanning confocal microscope (60X 1.4 NA air) was observed to be 600 ± 5 nm, 595 ± 5 nm and 525 ± 5 nm, respectively [117]. Figure 9 below shows the Siemen’s star test chart imaged using various techniques (previously described).

In order to improve the lateral resolution even further a structured illumination embedded speckle microscope was proposed and investigated. In a structured illumination embedded speckle microscopy, speckle patterns are embedded within the conventional illumination patterns used in SIM. Using a 50X NIKON TU Plan ELWD corrected long WD microscope objective (50X, NA 0.55, 11 mm WD) and a Siemen’s star chart as the test sample, a lateral resolution of ~ 310 ± 5 nm was achieved. In comparison to a conventional microscope (without the SIM unit and BBM unit) and an OS-SIM (without the BBM unit; using LCOS-SLM), the lateral resolution of a structured illumination embedded speckle microscope had improved by ~ 20% and ~ 48%, respectively. Further, to assess the image quality, two error metrics, namely, the mean square error and peak signal-to-noise ratio were used. A structured illumination embedded dynamic speckle microscopy was observed to improve the MSE and PSNR by ~ 45% and ~ 2.5 dB, respectively. Therefore, apart from improving the lateral resolution, the structured illumination embedded speckle microscopy was found to improve the quality of the image [118].

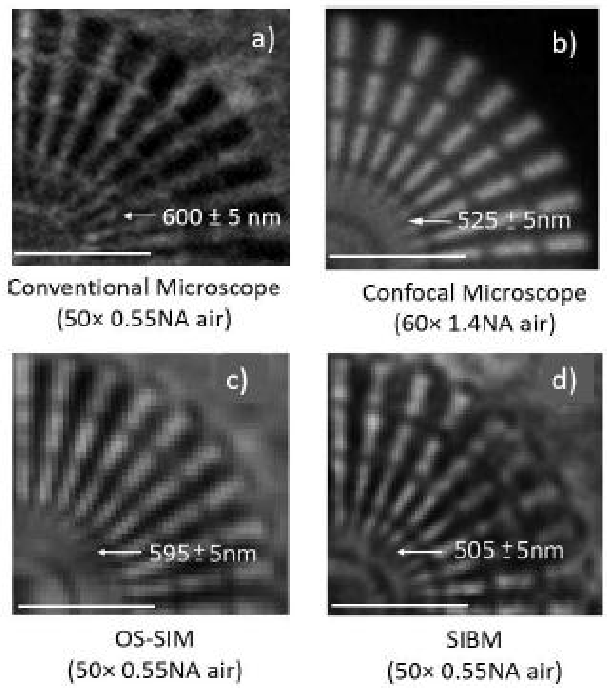

Fig 9. The Siemen's star image captured using (a) a conventional microscope, (b) a standard laser scanning confocal microscope (ZEISS, LSM 800 with a NIKON, high NA, short WD of 0.13 mm), (c) an OS-SIM and (d) SIBM. The white scale bar indicates 7.5 μm [8].

To fully understand the capability of a structured illumination embedded speckle microscopy, its axial response (optical sectioning ability) has also been assessed. The optical sectioning ability of a structured illumination embedded speckle microscope was estimated using a theoretical model and MATLAB® simulations. The optical sectioning ability of a microscope was experimentally validated using a 20X NIKON TU Plan ELWD corrected long WD microscope objective (20X, 0.4 NA, 19 mm WD) to obtain a larger FOV. Three samples, (i) a plane mirror, (ii) a Singapore 20 cent coin and (iii) a 3D printed sample were used for the tests. The plane mirror was scanned (axially) between z = – 6.5 μm to z = 6.5 μm (step size = 500 nm) and the normalized intensity was determined for every axial step. The samples are illuminated using the computationally generated binary sequence of correlated speckle patterns embedded within periodic gratings. The FWHM of the normalized intensity for a structured illumination embedded speckle microscopy was calculated to be 3 μm. In comparison, the FWHM of the normalized intensity for a confocal microscope (KEYENCE VK-x1000 laser confocal microscope using a 20X ELWD microscopic objective lens with a WD of 11 mm; 0.4 NA) and a speckle illumination microscope (without the SIM unit) was calculated to be 1 μm and 5 μm, respectively. Further, experiments on a Singapore 20 cent coin and a 3D printed sample confirm the improved optical sectioning ability of the proposed system. The sectioning ability of the proposed microscope is observed to be the maximum for, $\underline{\upsilon}$ = 0.4 and Δs = 5 pixels. As the value of $\underline{\upsilon}$ increases, the optical sectioning ability is improved [119].

All the above-mentioned techniques are being investigated for inspecting surface roughness of large structures. These techniques cannot be implemented for monitoring hard to access surfaces and internal channels. Therefore, a broader research activity was initiated to optimize and configure the developed techniques for such applications. To start with, various optical fiber-based probes for non-destructive evaluation of surface roughness parameters from difficult to access areas and internal channels (5 μm < Ra < 25 μm) have been developed and are being investigated. As a part of this investigation, optical fiber probes based on ASC and speckle image analysis were evaluated. The capability of these probes to evaluate surface roughness parameters were analyzed. By performing theoretical simulations using ZEMAX®, optical parameters of the probe based on ASC were optimized. A set of optimized geometrical parameters derived from the ZEMAX® simulations were used to configure the experimental arrangement. From the theoretical simulations and the experimental validations for the probe based on ASC, a measurement range of 5 μm < Ra < 25 μm was achieved. However, the following factors were observed to decrease the measurement repeatability, (a) the need to compensate for large measurement deviations for Ra ≥ 25 μm, (b) the dependence of the measurement accuracy on the optical alignment and (c) the complicated optical instrumentation [120,121].

In order to overcome these shortcomings, we also investigated optical fiber-based speckle imaging probes. A novel binary image analysis technique is used to evaluate the surface roughness parameters from the captured white light speckle images. Three algorithms, namely, frequency filtering, Gaussian filtering, and interpolation filtering, were investigated to remove the high frequency comb structures from the white light speckle images. The surface roughness parameters of three different ALM samples with build angles of 50, 550, and 750 were evaluated using the developed probe. A new parameter termed as the component connectivity exponent (CCE) is introduced to differentiate the surface topography of these samples. The CCE represents the exponential variation of the largest binary component with increasing values of threshold. The CCE measurements of the three ALM samples are validated using the MITUTOYO SJ-400 (conventional stylus probe) and the TALYSCAN 150 (optical stylus probe). The relationship between the CCE parameter and the surface roughness parameters obtained from the MITUTOYO SJ-400 (conventional stylus probe) and the TALYSCAN 150 (optical stylus probe) were analyzed. For the three samples, a similar trend was observed in the variation of CCE and the surface roughness parameters obtained from the MITUTOYO SJ-400 (conventional stylus probe) and the TALYSCAN 150 (optical stylus probe) (95% CI). Frequency filtering technique was observed to be useful in obtaining high frequency information from the white light speckle images compared to the Gaussian filtering and the interpolation filtering techniques. In the case of Gaussian filtering and interpolation filtering, the high frequency components of the surface scatter were filtered. This led to a positive drift in the measured value of CCE, especially for the samples with the 550 and 750 build angles. The variation of CCE values was seen to be attributed to three main factors, the comb structure removal algorithm used, the sample tilt and the surface roughness parameter. Lastly, the time taken for calculating the CCE parameter using an optical fiber-based speckle imaging probe (~ 130 seconds) was found to be less than by conventional TALYSCAN 150 instrument (~ 860 seconds) [122].

4 Conclusion

Measurement of surface roughness parameters, from futuristic aircraft engine components having large surface areas with micro-scale features and components located at areas hard to access, was identified as a metrological challenge. The average surface roughness, Ra for the components having large surface areas, was identified to vary between 0.2 μm and 0.6 μm. Alternatively, for the components located at difficult to access areas or contain complex internal channels, the Ra was identified to vary between 5 μm and 25 μm.

The currently available techniques to evaluate the surface roughness parameters of components having large surface areas with micro-scale features include a stylus, SEM, AFM, and optical microscopy.

Even though surface roughness parameters can be extracted from the high-resolution surface images obtained from these techniques, they are limited by their inability to adhere to industrial requirements such as the scanning speed, FOV, and the influence of an industrial environment. In this context, speckle-based techniques, including speckle contrast, speckle correlation, and speckle imaging, were investigated. The advantages offered by speckle-based techniques for surface roughness evaluation include full field instantaneous data acquisition, high measurement speed, and the possibility of measuring surfaces with higher angular slopes. Although speckle-based surface roughness evaluation is well established, the measurement range of these techniques has not been investigated. Further, the relationship between speckle statistics and areal surface roughness parameters is not established. Also, the areal roughness parameters extracted from speckle statistics may slightly differ from the ones measured by the conventional line and areal inspection techniques. Therefore, to overcome these disadvantages, techniques that evaluate the real surface topography (in-line with industry 4.0) to determine the surface roughness parameters were investigated.

A real surface topography evaluation techniques could be divided into, (i) interferometry- based, (ii) deflectometry-based and (iii) triangulation-based techniques depending upon the principles of operation, the dominant source of noise and measurement uncertainties. Even though interferometric techniques including CSI (or WLI), PSI and DHM have been used for high resolution surface topography measurements, they are limited by the phase errors and speckle noise. PSI, being vastly implemented for 2D surface roughness evaluation, are not used for 3D topography measurements and require an additional reference surface. On the other hand, commercially available DHM systems are capable of high precision measurements at about 20 fps. However, these benchtop systems are limited due to speckle noise while characterizing the rough surfaces. In contrast, high-resolution deflectometry-based techniques for surface topography evaluation determine the slope of the surface under inspection. Although this technique can be used to generate SEM-like surface topography images, the FOV is limited to 100 μm. Along with the interferometry and deflectometry-based techniques, triangulation-based systems have also been widely used for surface roughness evaluation. Techniques including focus variation microscopy and confocal microscopy are commercially available systems that can evaluate high-resolution 3D images of the sample surface. However, these systems are limited by the diffraction limits of the objective lenses used. Hence, for evaluating high-resolution surface topography images, a microscopic objective with a high NA is mandated. The choice of a high NA objective lens implies, (i) a smaller WD, (ii) a smaller FOV, and (iii) errors due to surface slopes. Techniques including SIM have been employed to image beyond the diffraction limit of the microscopic objective lens. Although SIM is a well-established technique for diffraction limited imaging of biological samples, very few studies were reported about their implementation on technical surfaces [93-98]. Also, methods to improve the capability of SIM for inspecting technical surfaces have not been investigated. In summary, the currently available techniques are incapable of evaluating the surface roughness parameters from a large FOV, long WD at high speeds. Considering the potential and significance of surface roughness on the aerodynamic and structural efficiency of an aircraft engine, techniques that challenge the fundamental limitations of optics must be investigated.

For the components located at areas hard to access and internal channels, none of the currently available techniques including conventional stylus probes, rigid borescopes, and flexible borescopes meet the requirements of quantitative data evaluation. Even though the physical limitations of the rigid probes can be solved by using optical fiber-based probes, none of the miniaturized systems currently available are capable of meeting the surface roughness measurement requirements. In this context, a miniaturized fiber probe for a fast, non-destructive, and non-contact surface roughness measurement is envisaged.

Acknowledgements

The authors acknowledge the financial support received from "COLE-EDB and ACRF RG 192/17 (MOE Singapore)". This work was carried out when Aswin Haridas was pursuing Ph D at the School of

MAE, NTU Singapore. He acknowledges NTU Singapore for the research scholarship received through the NTU - RSS scheme.

References

1. Changi Group. (2019, January 29). Traffic Statistics. Retrieved from http://www.changiairport.com/corporate/our-expertise/air-hub/traffic-statistics.html.
2. Boston Consulting Group. Embracing Industry 4.0 and Rediscovering Growth. Describes the 9 pillars of industry 4.0. Retrieved from: www.bcg.com/capabilities/operations/embracing-industry-4.0-rediscovering-growth.aspx.
3. Backman D G, Williams J C, Advanced materials for aircraft engine applications, *Science*, 255(1992)1082–1087.
4. Red C, Composites in commercial aircraft engines, 2014-2023. Retrieved from: http://www.compositesworld.com/articles/composites-in-commercial-aircraft-engines-2014-2023.
5. Hartl D J, Lagoudas D C, Aerospace applications of shape memory alloys. Proceedings of the Institution of Mechanical Engineers, Part G: *J Aerosp Eng*, 221(2007)535–552.
6. Bheekhun N, Talib A, Rahim A, Hassan M R, Aerogels in aerospace: an overview, *Adv Mater Sci Eng*, (2013) Article ID 406065; doi.org/10.1155/2013/406065.
7. Leach R, Sherlock B, Applications of super-resolution imaging in the field of surface topography measurement. *Surf Topogr: Metrol Prop*, 2(2013)023001; doi.10.1088/2051-672X/2/2/023001.
8. Haridas A, Investigation into micro and nano scale optical metrology for shiny surfaces and difficult to access aircraft engine components. Doctoral Thesis, Nanyang Technological University, Singapore, 2019.
9. Leach R, Chapter 1 - Introduction to Metrology for Advanced Manufacturing and Micro- and Nanotechnology, in Fundamental Principles of Engineering Nanometrology, 2nd Edn, (William Andrew Publishing: Oxford), 2014, p. 1-6.
10. Leach R, Chapter 1 - Optical Measurement of Surface Topography, electronic resource, (Springer-Verlag Berlin Heidelberg), 2011, pp 1-14.
11. Amra C, Torricini D, Roche P, Multiwavelength (0.45–10.6 μm) angle-resolved scatterometer or how to extend the optical window, *Appl Opt*, 32(1993)5462–5474.
12. Roche P, Pelletier E, Characterizations of optical surfaces by measurement of scattering distribution, *Appl Opt*, 23 (1984)3561–3566.
13. Watkins S E, Black J P, Pond B J, Optical scatter characteristics of high-reflectance dielectric coatings and fused-silica substrates, *Appl Opt*, 32(1993)5511–5518.
14. Kienzle O, Staub J, Tschudi T, Light scattering from transparent substrates: theory and experiment, *Phys Rev B*, 50(1994)1848–1860.
15. Gliech S, Steinert J, Duparré A Light-scattering measurements of optical thin-film components at 157 and 193 nm. *Appl Opt*, 41(2002)3224–3235.
16. Lequime M, Zerrad M, Deumié C, Amra C, A goniometric light scattering instrument with high-resolution imaging, *Opt Commun,* 282(2009)1265–1273.
17. Hou H, Yi K, Shang S, Shao J, Fan Z, Measurements of light scattering from glass substrates by total integrated scattering, *App Opt*, 44(2005)6163–6166.
18. Tay C J, Wang S H, Quan C, Ng B L, Chan K C, Surface roughness investigation of semi-conductor wafers, *Opt Laser Technol*, 36(2004)535–539.
19. Mazule L, Liukaityte S, Eckardt R C, Melninkaitis A, Balachninaite O, Sirutkaitis V, A system for measuring surface roughness by total integrated scattering, *J Phys D: Appl Phys*, 44(2011)505103; doi.10.1088/0022-3727/44/50/505103.
20. Jakobs S, Duparre A, Truckenbrodt H, AFM and light scattering measurements of optical thin films for applications in the UV spectral region, *Int J Mach Tools Manuf*, 38(1998)733–739.
21. Amra C, Grezes-Besset C, Roche P, Pelletier E, Description of a scattering apparatus: application to the problems of characterization of opaque surfaces, *Appl Opt*, 28(1989)2723–730.
22. Schröder S, Gliech S, Duparré A, Measurement system to determine the total and angle-resolved light scattering of optical components in the deep-ultraviolet and vacuum-ultraviolet spectral regions, *Appl Opt*, 44(2005)6093–6107.

23. Elson J M, Rahn J P, Bennett J M, Relationship of the total integrated scattering from multilayer-coated optics to angle of incidence, polarization, correlation length, and roughness cross-correlation properties, *Appl Opt*, 22 (1983)3207–3219.
24. Stover J C, Optical scattering. Measurement and analysis, (SPIE Press Volume), 1995, p. 85-109.
25. Briers J D, Surface roughness evaluation. In: Speckle metrology, (CRC Press), 2020, p. 373-426.
26. Fujii H, Asakura T, Roughness measurements of metal surfaces using laser speckle, *J Opt Soc Am*, 67(1977)1171–1176.
27. Goodman J W, Some fundamental properties of speckle, *J Opt Soc Am*, 66(1976)1145–1150.
28. Salazar F, Barrientos A, Surface roughness measurement on a wing aircraft by speckle correlation, *Sensors*, 13 (2013)11772–11781.
29. Toh S L, Shang H M, Tay C J, Surface-roughness study using laser speckle method, *Opt Lasers Eng*, 29(1998)217–225.
30. Briers J D, Chapter 3- Surface roughness evaluation, In: Speckle Metrology, Sirohi R S, (Marcel Dekker. New York), 1993, p. 373-418.
31. Erf R, Speckle metrology, (New York: Academic Press), 1978, p. 11-49.
32. Burch J M, Laser speckle metrology. In: Developments in Holography II, International Society for Optics and Photonics, 1971, p. 149-156.
33. Corrêa R D, Meireles J B, Huguenin J A O, Caetano D P, Da Silva L, Fractal structure of digital speckle patterns produced by rough surfaces, *Phys A: Stat Mech Appl*, 392(2013)869–874.
34. Dhanasekar B, Mohan N K, Bhaduri B, Ramamoorthy B, Evaluation of surface roughness based on monochromatic speckle correlation using image processing, *Precis Eng*, 32(2008)196–206.
35. Ettl P, Schmidt B E, Schenk M, Laszlo I, Haeusler G, Roughness parameters and surface deformation measured by coherence radar, In: International Conference on Applied Optical Metrology, 3407(1998)133–140.
36. Hamed A M, El-Ghandoor H, El-Diasty F, Saudy M, Analysis of speckle images to assess surface roughness, *Opt Laser Technol*, 36(2004)249–253.
37. Persson U, Surface roughness measurement on machined surfaces using angular speckle correlation, *J Mater Process Technol*, 180(2006)233–238.
38. Matham M V, Seng O L, Asundi A, Polarization phase shifting shearography for optical metrological applications, *Opt Laser Techno*, 30(1998)527–531.
39. Matham M V, Narayanan Unni S, Digital speckle pattern interferometry for deformation analysis of inner surfaces of cylindrical specimens, *Appl Opt*, 43(2004)2400–2408.
40. Goodman J W, Dependence of image speckle contrast on surface roughness, *Opt Commun*, 14(1975)324–327.
41. Persson U, Real time measurement of surface roughness on ground surfaces using speckle-contrast technique, *Opt Lasers Eng*, 17(1992)61–67.
42. Leonard L C, Toal V, Roughness measurement of metallic surfaces based on the laser speckle contrast method, *Opt Lasers Eng*, 30(1998)433–440.
43. Persson U, Measurement of surface roughness on rough machined surfaces using spectral speckle correlation and image analysis, *Wear*, 160(1993)221–225.
44. Léger D, Mathieu E, Perrin J C, Optical surface roughness determination using speckle correlation technique, *Appl Opt*, 14(1975)872–877.
45. Spagnolo G S, Paoletti D, Paoletti A, Ambrosini D, Roughness measurement by electronic speckle correlation and mechanical profilometry, *Measurement*, 20(1997)243–249.
46. Toh S L, Quan C, Woo K C, Tay C J, Shang H M, Whole field surface roughness measurement by laser speckle correlation technique, *Opt Laser Techno*, 33(2001)427–434.
47. Ruffing B, Application of speckle-correlation methods to surface-roughness measurement: a theoretical study, *J Opt Soc Am A*, 3(1986)1297–1304.
48. Ruffing B, Fleischer J, Spectral correlation of partially or fully developed speckle patterns generated by rough surfaces, *J Opt Soc Am A*, 2(1985)1637–1643.

49. Spagnolo G S, Cozzella L, Leccese F, Viability of an optoelectronic system for real time roughness measurement, *Measurement*, 58(2014)537–543.
50. Schreiber H, Bruning J H, Phase shifting interferometry, Optical shop testing, (Wiley Interscience, Hoboken, NJ), Ch 14, (2007), pp 547–666.
51. Neuschaefer-Rube U, Neugebauer M, Ehrig W, Bartscher M, Hilpert U, Tactile and optical microsensors: test procedures and standards, *Meas Sci Technol*, 19(2008)084010; doi.org/10.4028/www.scientific.net/KEM.381-382.23
52. Vargas J, Quiroga J A, Belenguer T, Phase-shifting interferometry based on principal component analysis, *Opt Lett*, 36(2011)1326–1328.
53. O'Mahony C, Hill M, Brunet M, Duane R, Mathewson A, Characterization of micromechanical structures using white-light interferometry, *Meas Sci Technol*, 14(2003)1807; doi.10.1088/0957-0233/14/10/310.
54. Lee B S, Strand T C, Profilometry with a coherence scanning microscope, *Appl Opt*, 29(1990)3784–3788.
55. Kaplonek W, Lukianowicz C, Coherence correlation interferometry in surface topography measurements, Recent Interferometry Applications in Topography and Astronomy, *Intech Open*, (2012)1-26.
56. Lee-Bennett, Advances in non-contacting surface metrology, In: Optical Fabrication and Testing, Optical Society of America, (2004), p OTuC1; doi. 10.1364/OFT.2004.OTuC1.
57. De Nicola S, Ferraro P, Grilli S, Miccio L, Meucci R, Buah-Bassuah P. K, Arecchi F. T, Infrared digital reflective-holographic 3D shape measurements, *Opt commun*, 281(2008)1445–1449.
58. Pedrini G, Zhang F, Osten W, Digital holographic microscopy in the deep (193 nm) ultraviolet, *Appl Opt*, 46 (2007)7829–7835.
59. Kim M K, Principles and techniques of digital holographic microscopy, *SPIE Rev*, 1(2010)018005; doi. 10.1117/6.0000006.
60. Kühn J, Charrière F, Colomb T, Cuche E, Montfort F, Emery Y, Depeursinge C, Axial sub-nanometer accuracy in digital holographic microscopy, *Meas Sci Technol*, 19(2008)074007; doi. 10.1088/0957-0233/19/7/074007.
61. Kühn J, Colomb T, Montfort F, Charrière F, Emery Y, Cuche E, Marquet P, Depeursinge C, Real-time dual-wavelength digital holographic microscopy with a single hologram acquisition, *Opt Express*, 15(2007)7231–7242.
62. Ritter R, Hahn R, Contribution to analysis of the reflection grating method, *Opt Lasers Eng*, 4(1983)13–24.
63. Knauer M C, Kaminski J, Hausler G, Phase measuring deflectometry: a new approach to measure specular free-form surfaces, In Optical Metrology in Production Engineering, International Society for Optics and Photonics, (2004), p. 366-376.
64. Bothe T, Li W, von Kopylow C, Juptner W P, High-resolution 3D shape measurement on specular surfaces by fringe reflection, In Optical Metrology in Production Engineering, International Society for Optics and Photonics, (2004), p. 411-422.
65. Höfer S, Burke J, Heizmann M, Infrared deflectometry for the inspection of diffusely specular surfaces, *Adv Opt Technol*, 5(2016)377–387.
66. Butel G P, Smith G A, Burge J H, Deflectometry using portable devices, *Opt Eng*, 54(2015)025111;doi. 10.1117/1.OE.54.2.025111.
67. Häusler G, Richter C, Leitz K H, Knauer M C, Microdeflectometry—a novel tool to acquire three-dimensional microtopography with nanometer height resolution, *Opt Lett*, 33(2008)396–398.
68. Haeusler G, U.S. Patent No. 8,224,066. Washington, DC: U.S. Patent and Trademark Office, 2012.
69. Häusler G, Vogel M, Yang Z, Kessel A, Faber C, Kranitzky C, Microdeflectometry and structural illumination microscopy–new tools for 3D-metrology at nanometer scale. In Proc Precision Interferometric Metrology, ASPE 2010 Summer Topical Meeting, Asheville, North Carolina, USA, (2010), p. 46-51.
70. Dorsch R G, Häusler G, Herrmann J M, Laser triangulation: fundamental uncertainty in distance measurement, *Appl Opt*, 33(1994)1306–1314.
71. Dresel T, Häusler G, Venzke H, Three-dimensional sensing of rough surfaces by coherence radar, *Appl Opt*, 31 (1992)919–925.
72. Häusler G, Ettl S, Limitations of optical 3D sensors. In Optical measurement of surface topography, (Springer, Berlin, Heidelberg), 2011, pp 23-48.

73. Danzl R, Helmli F, Form measurement of engineering parts using an optical measurement system based on focus variation, In 7th European Society for Precision Engineering and Nanotechnology International Conference, (2007)
74. Danzl R, Helmli F, Scherer, S,Focus variation–a new technology for high resolution optical 3D surface metrology, In The 10th international conference of the slovenian society for non-destructive testing, (2009), p. 484-491.
75. Minsky M, Memoir on inventing the confocal scanning microscope, *Scanning*, 10(1988)128–138.
76. Leach R K , Fundamental principles of engineering nanometrology. [electronic resource]. Micro and nano technologies, (Oxford : William Andrew ; Amsterdam : Elsevier Science), 2010, pp 263–288.
77. Jordan H J, Wegner M, Tiziani H, Highly accurate non-contact characterization of engineering surfaces using confocal microscopy, *Meas Sci Technol*, 9(1998)1142; doi. 10.1088/0957-0233/9/7/023.
78. Hamilton D K, Wilson T, Three-dimensional surface measurement using the confocal scanning microscope, *Appl Phys B*, 27(1982)211–213.
79. Wilson T, Resolution and optical sectioning in the confocal microscope, *J Microsc*, 244(2011)113–121.
80. Carlsson K, Åslund N, Confocal imaging for 3-D digital microscopy, *Appl Opt*, 26(1987)3232–3238.
81. Hamilton D K, Wilson T, Three-dimensional surface measurement using the confocal scanning microscope, *Appl Phys B*, 27(1982)211–213.
82. Zhang Y, Strube S, Molnar G, Danzebrink H U, Dai G, Bosse H, Hou W, Parallel large-range scanning confocal microscope based on a digital micromirror device, *Optik*, 124(2013)1585–1588.
83. Petráň M, Hadravský M, Boyde A, The tandem scanning reflected light microscope, *Scanning*, 7(1985)97–108.
84. Martial F P, Hartell N A, Programmable Illumination and High-Speed, Multi-Wavelength, Confocal Microscopy Using a Digital Micromirror, *PLoS ONE*, 7(2012) e43942; doi.org/10.1371/journal.pone.0043942.
85. Engelhardt K, Häusler G, Acquisition of 3-D data by focus sensing, *Appl Opt*, 27(1988)4684–4689.
86. Wilson T, Neil M A A, Juskaitis, R, U.S. Patent No. 6,376,818. Washington, DC: U.S. Patent and Trademark Office, 2002.
87. Gustafsson M G, Shao L, Carlton P M, Wang C R, Golubovskaya I N, Cande W Z, Sedat J W, Three-dimensional resolution doubling in wide-field fluorescence microscopy by structured illumination, *Biophys J*, 94 (2008)4957–4970.
88. Gustafsson M G, Nonlinear structured-illumination microscopy: wide-field fluorescence imaging with theoretically unlimited resolution, *Proceedings of the National Academy of Sciences*,(USA),102(2005)13081–13086.
89. Gustafsson M G, Surpassing the lateral resolution limit by a factor of two using structured illumination microscopy, *J Microsc*, 198(2000)82–87.
90. Heintzmann R, Structured illumination methods. In: Handbook of biological confocal microscopy, (Springer, Boston, MA), 2006, pp. 265-279
91. Dan D, Yao B, Lei M, Structured illumination microscopy for super-resolution and optical sectioning, *Sci Bull*, 59(2014)1291–1307.
92. Heintzmann R, Huser T, Super-resolution structured illumination microscopy, *Chem Rev*, 117(2017)13890–13908.
93. Häusler G, Vogel M, Yang Z, Kessel A, Faber C, SIM and deflectometry: new tools to acquire beautiful, SEM-like 3D images. In Imaging Systems and Applications, Optical Society of America, (2011), p. JWC1.
94. Vogel M, Kessel A, Yang Z, Faber C, Seraphim M C, Häusler G, Tuning structured illumination microscopy (SIM) for the inspection of micro optical components. In Proc DGaO, (2010), p A22.
95. Vogel M, Yang Z, Kessel A, Kranitzky C, Faber C, Häusler G, Structured-illumination microscopy on technical surfaces: 3D metrology with nanometer sensitivity, In Optical Measurement Systems for Industrial Inspection VII, International Society for Optics and Photonics, (2011), p. 80820S.
96. Kranitzky C, Richter C, Faber C, Knauer M C, Häusler G, 3D-microscopy with large depth of field. In DGaO Proceedings, (2009), p A12.
97. Yang Z, Bielke A, Häusler G, Better three-dimensional inspection with structured illumination: speed, *Appl Opt*, 55(2016)1713–1719.
98. Yang Z, Kessel A, Häusler G, Better 3D inspection with structured illumination: signal formation and precision, *Appl Opt*, 54(2015)6652–6660.

99. Saxena M, Eluru G, Gorthi S S, Structured illumination microscopy, *Adv Opt Photonics*, 7(2015)241–275.
100. Xu J J, Lee K K, 3-d optical microscope. U.S. Patent No.20100135573A1, Washington, DC: U.S. Patent and Trademark Office, 2010.
101. Flusberg B A, Cocker E D, Piyawattanametha W, Jung J C, Cheung E L, Schnitzer M J, Fiber-optic fluorescence imaging, *Nat Methods,* 2(2005)941–950.
102. Yamazaki K, U.S. Patent No. 5,757,496. Washington, DC, U.S. Patent and Trademark Office, 1998.
103. Xu X, Liu S, Hu H, A new fiber optic sensor for inner surface roughness measurement, In 2009 International Conference on Optical Instruments and Technology: Advanced Sensor Technologies and Applications, International Society for Optics and Photonics, (2009), p. 75080J.
104. Smith M D, Fibre interferometry for differential measurements, Doctoral dissertation, Engineering and Physical Sciences, Heriot-Watt University, Edinburgh, Scotland, 2015.
105. Steelman Z A, Kim S, Jelly E T, Crose M, Chu K K, Wax A, Comparison of imaging fiber bundles for coherence-domain imaging, *Appl Opt*, 57(2018)1455–1462.
106. Xie T, Mukai D, Guo S, Brenner M, Chen Z, Fiber-optic-bundle-based optical coherence tomography, *Opt Lett,* 30(2005)1803–1805.
107. Gmitro A F, Aziz D, Confocal microscopy through a fiber-optic imaging bundle, *Opt Lett*, 18(1993)565–567.
108. Kobayashi T, Shan X C, Murakoshi Y, Maeda R, A novel self-sensitive SFM for nondestructive measurement of tiny vertical surfaces with restricted access, In Symposium on Design, Test, Integration and Packaging of MEMS/MOEMS 2003, IEEE, (2003), p. 286-289.
109. Prabhathan P, Song C, Haridas A, Prasad G, Chan K, Intensity and contrast based surface roughness measurement approaches for rough and shiny surfaces, In Fifth International Conference on Optical and Photonics Engineering, International Society for Optics and Photonics, (2017), p. 1044912.
110. Dev K, Prasad G, Haridas A, Prabhathan P, Chan K H, Matham M V, Surface roughness measurement of additive manufactured samples using angular speckle correlation, In Fifth International Conference on Optical and Photonics Engineering, International Society for Optics and Photonics, (2017), p. 104492W.
111. Prabhathan P, Song C, Haridas A, Prasad G, Chan K, Murukeshan V M, Experimental investigations and parametric studies of surface roughness measurements using spectrally correlated speckle images, In Fifth International Conference on Optical and Photonics Engineering, International Society for Optics and Photonics, (2017), p. 1044913.
112. Haridas A, Prabhathan P, Pulkit K, Chan K, Murukeshan V M, Surface roughness mapping of large area curved aerospace components through spectral correlation of speckle images, *Appl Opt*, 59(2020)5041–5051.
113. Matham M, Prabhathan P, Haridas A, Kapur P, Bilal NM; Chan KHK, Non-contact surface roughness map display on large area curved samples, European Patent Application No. 19216655.1, EP3680607A1, Date filed: 08 Jan 2019.
114. Haridas A, Crivoi A, Patinharekandy P, Chan K, Murukeshan V M, Fractal speckle image analysis for surface characterization of aerospace structures. In Fifth International Conference on Optical and Photonics Engineering, International Society for Optics and Photonics (2017), p. 104491T
115. Haridas A, Crivoi A, Patinharekandy P, Chan K, Murukeshan V M, A fractal image analysis methodology for heat damage inspection in carbon fiber reinforced composites, In Fifth International Conference on Optical and Photonics Engineering, International Society for Optics and Photonics (2017), p. 104491L
116. Matham M, Haridas A, Crivoi A, Prabhathan P, Determining Surface Roughness, , UK Patent Application No. GBGB1705406.5A, Date filed: 04 Apr 2017.
117. Perinchery S M, Haridas A, Shinde A, Buchnev O, Murukeshan V M, Breaking diffraction limit of far-field imaging via structured illumination Bessel beam microscope (SIBM), *Opt Express*, 27(2019)6068–6082.
118. Haridas A, Perinchery S M, Shinde A, Buchnev O, Murukeshan V M, Long working distance high resolution reflective sample imaging via structured embedded speckle illumination, *Opt Lasers Eng*, 134(2020)106296; doi. 10.1016/j.optlaseng.2020.106296.
119. Haridas A, Matham M, Enhancing the limits of optical sectioning in far field reflection microscopy , *Opt Lasers Eng*,(Submitted), 2021.

120. Subbarao G P A, Haridas A, Patinharekandy P, Kapur P, Chan K, Flexible optical fiber probe for surface roughness evaluation of internal channels in additively manufactured components, Proceedings of the 3rd International Conference on Progress in Additive Manufacturing, Pro-AM (2018), p. 601-606. https://doi:10.25341/D4NK5F

121. Matham M, Chan K, Subbarao GPA, Prabhathan P, Haridas A, Kapur P, Measuring surface roughness, UK Patent Application No. 1718699.0, GB201718699D0, United Kingdom, Date filed: 13 Nov 20171718699.0; 27 Nov 2017.

122. Haridas A., Matham M V, Crivoi A, Patinharekandy P, Jen T M, Chan K, Surface roughness evaluation of additive manufactured metallic components from white light images captured using a flexible fiberscope, *Opt Lasers Eng*, 110(2018)262–271.

[*Received*: 03.09.2021; *accepted*: 01.10.2021]

Dr Aswin Haridas is currently with Structural Health Monitoring (SHM) at Testia GmbH, an Airbus company located at Bremen, Germany. He completed his Ph D, which was focused on developing new inspection capabilities and strategies for critical aircraft engine structures, at Nanyang Technological University (NTU), Singapore in collaboration with Rolls-Royce Singapore. Prior to this, he had pursued his masters (M Sc) in Aerospace Structural Engineering as a joint degree program between Technische Universität München (TUM) and NTU. He has over 8 years of R&D experience in identifying and developing Non-Destructive Testing (NDT) and Structure health Monitoring (SHM) solutions for industries including aerospace, automotive, civil and energy (among many others). He has published a number of articles in Internationally Recognized Journals and Conferences and holds Five, UK registered Patents on Surface Inspection Techniques of Aircraft Engine Components.

Prof Murukeshan Vadakke Matham is working at the Centre for Optical and Laser Engineering (COLE), Nanyang Technological University (NTU), Singapore. He has more than 25 years of professional experience. His basic background is in Physics (Optics) with strong interdisciplinary research expertise and interest in the areas of Nanoscale Optics and Biomedical Optics. He has 23 patents that are either filed, patented or assigned to MNCs and that have attracted significant amount of innovation and potential industry funding. He has published over 200 papers in archival journals, and more than 180 conference proceedings papers/presentations. He is the Associate Editor of two leading SCI indexed international journals such as Optical Engineering and IJO, and also on the editorial board of NPG publication. He has achieved many recognitions in his career which includes DAAD Fellowship (Germany), Singapore prime ministers Technology Challenge Award, TCT Exchange Fellowship, MEXT Visiting Researcher Japan, Rolls Royce Innovator Award, to name a few. He was also awarded Erudite Professorship. He is Fellow SPIE (USA), Fellow OPTICA (USA), Fellow Institute of Physics (UK), and Distinguished fellow of Optical society of India (OSI).

He is currently serving as the Director of Centre for Optical & Laser Engineering (COLE), and Deputy Director of The Photonics Institute (TPI), NTU. He leads a research group which focuses on cutting-edge research and development based on physics (optics) in the areas of Biomedical Optics, Nanoscale Optics, Laser-based Micro and Nanoscale Fabrication, and Applied Optics for Metrology.